The Penetration of Solar Radiation into Water and Carbon Dioxide Snow, with reference to Mars

JGR Planets

RESEARCH ARTICLE
10.1029/2018JE005771

The Penetration of Solar Radiation Into Water and Carbon Dioxide Snow, With Reference to Mars

H. E. Chinnery[1], A. Hagermann[2], E. Kaufmann[2], and S. R. Lewis[1]

[1]School of Physical Sciences, The Open University, Milton Keynes, UK, [2]Department of Biological and Environmental Sciences, University of Stirling, Stirling, UK

Abstract The depth to which solar radiation can penetrate through ice is an important factor in understanding surface-atmosphere interactions for icy planetary surfaces. Mars hosts both water and carbon dioxide ice on the surface and in the subsurface. At high latitudes during autumn and winter carbon dioxide condenses to form the seasonal polar cap. This has been both modeled and observed to, in part, occur as snowfall. As snow accumulates, the thermal properties of the surface are changed, whether the underlying surface was rocky, regolith, or a solid ice sheet. This results in a change (usually increase) in albedo, affecting the proportion of the incident solar energy reflected, or transmitted below the surface of the snow layer. The depth to which light can penetrate through this layer is an important parameter in heat transfer models for the Martian surface and is often quantified using the *e*-folding scale. We present the first measurements of the *e*-folding scale in pure carbon dioxide snow for the wavelengths 300 to 1100 nm alongside new measurements of water snow.

Plain Language Summary The solid-state greenhouse effect is similar to the climatic greenhouse effect. It occurs in solid materials that are translucent to visible light, but opaque in the infrared, such as ices. On Mars, snow and frosts form from both water and carbon dioxide ice. When the Sun shines on the snow or frost, some light is diffusely reflected, some is transmitted through the snow grains, and some is absorbed by the ice. The proportion of light that travels through a material is dependent on its optical properties, which are unique to its composition. Owing, however, to the nature of frost or snow being a very small, granular material, much of the light is scattered at the grain surfaces. In this study we measured the amount of light that can travel through a snowpack of a particular thickness for both water and carbon dioxide snows. This helps determine how much energy can be transported through the snow to the ground below, which warms up the underlying material. This means that more accurate calculations can be made about the temperature profile of the Martian surface when covered in snow and frost, which gives insight into the different surface processes observed on Mars.

Key Points:
- The *e*-folding scale for fresh snow is found to be 11 ± 3 mm regardless of composition (water or carbon dioxide)
- In a snowpack, light propagation is dominated by scattering at grain surfaces instead of transmission through the ice itself

Supporting Information:
- Supporting Information S1

Correspondence to:
H. E. Chinnery,
hannah.chinnery@open.ac.uk

Citation:
Chinnery, H. E., Hagermann, A., Kaufmann, E., & Lewis, S. R. (2019). The penetration of solar radiation into water and carbon dioxide snow, with reference to Mars. *Journal of Geophysical Research: Planets*, *124*. https://doi.org/10.1029/2018JE005771

Received 26 JUL 2018
Accepted 17 JAN 2019
Accepted article online 21 JAN 2019

1. Introduction

Mars' northern permanent polar cap consists mostly of water ice, whereas the southern cap has a stable layer of carbon dioxide ice overlying the water ice. Carbon dioxide constitutes approximately 95% of the atmosphere of Mars, with water vapor constituting only 0.03% (Gillmann et al., 2009). During winter, the atmospheric pressure can drop by up to 25% (e.g., Leighton & Murray, 1966; Snyder, 1979), which equates to around 12–16% of the atmosphere by mass (Genova et al., 2016) due to the growth of the seasonal polar caps, which form expansive sheets of CO_2 ice. This ice can be emplaced by two different methods: precipitation or direct condensation.

Based on observations by the Mars Climate Sounder, Hayne et al. (2014) developed models which show snowfall contributes between 3% and 20% by mass to the southern seasonal ice deposits at latitudes ranging from 70°S to 90°S, with the rest condensing directly from the atmosphere to the surface by radiative cooling. A number of previous studies had inferred CO_2 snow fall to be a common occurrence during the Martian winter, such as Titus et al. (2001), Hayne et al. (2012), and Kuroda et al. (2013). In addition to this, Piqueux et al. (2016) reported widespread CO_2 frost deposits based on observations by the Mars Climate Sounder on board the Mars Reconnaissance Orbiter, significant due to the latitudinal range over which the frosts were found, which reached into equatorial regions of low surface thermal conductivity and high elevation, such as around Tharsis Rise. This shows the CO_2 condensation-sublimation cycle affects the surface on a global scale and is not just confined to high latitudes. These environments may be short-lived

—microphysical models suggest that surface sintering could occur rapidly, removing particles less than 1 mm in a matter of days (Clark et al., 1983; Eluszkiewicz, 1993; Eluszkiewicz et al., 2005), although small-grained deposits are observed for longer periods, and so thought to be the locations of frequent snowfall (Hayne et al., 2012). Additionally, water snow fall and ice formation has been observed, in this instance directly, by the Phoenix Lander during late summer at its landing site (68.22 N, 125.70 W), before being covered by the seasonal polar cap of CO_2 ice (e.g., Cull et al., 2010; Smith et al., 2009).

The Phoenix Lander also observed nighttime water snow and ground frosts during late summer (Smith et al., 2009) at its landing site of 68.22° latitude in northern polar region (Arvidson et al., 2009; Smith et al., 2009). This increased in duration and quantity through to the end of Phoenix's operating period, and orbital measurements show this was followed by CO_2 ice coverage at approximately 30 cm deep (Cull et al., 2010), increasing in thickness poleward to around 1 m.

For the purposes of this investigation, "snow" is used to describe fine-grained or porous ice deposits, of either H_2O or CO_2 ice. This could therefore be representative of both snowfall and surface frosts. Kaufmann and Hagermann (2015) and France et al. (2010) conducted experiments to determine the *e*-folding scale of water snow, and the effect of adding Mars simulant dust to the snow, using different methodologies, resulting in *e*-folding scales for pure water snow an order of magnitude different. What neither of these studies addressed, however, is how the presence of CO_2 snow, rather than water snow, affects the light penetration depth within Martian snowpacks.

Here we investigate the *e*-folding scale of snow, composed of both H_2O and CO_2 ices, in order to determine how the presence of CO_2 snow affects surface processes which are driven by the interaction of solar irradiation with a surface. It is also important to have accurate and consistent water snow measurements, made under the same conditions, in order for direct comparisons to be made. Warren (1982) stressed the importance of understanding the optical properties of snow for calculating the radiation budget for snow-covered surfaces, in addition to applications for the remote sensing of snow-covered planetary surfaces. Ices behave differently to rocky or regolith-covered surfaces when exposed to solar irradiation because ices are translucent or transparent to visible and shorter wavelengths of light, while being opaque in the infrared. These properties contribute to the solid-state greenhouse effect (SSGE), first described by Matson and Brown (1989), although the concept that subsurface temperatures could be higher than the surface temperature in a terrestrial snowpack was reported first by Niederdorfer (1933). The extent of the SSGE is determined by multiple factors, including the optical properties of the icy material, grain size and shape, impurities, and depth of ice. One of the most important, but poorly understood, parameters when quantifying the SSGE is the *e*-folding scale (ζ), or penetration depth, of solar radiation within the sample (Möhlmann, 2010). Using the *e*-folding scale, the downward directed energy flux (F), as a function of ice thickness (x), is expressed as

$$F(x) = e^{-x/\zeta} \tag{1}$$

Carbon dioxide ice has very different optical properties to water ice. The latter absorbs strongly throughout the infrared, whereas CO_2 ice absorbs strongly in only three narrow bands in the midinfrared ($\lambda < 25$ μm), and two lattice absorptions in the far infrared ($\lambda > 25$ μm), with only very weak absorption in between these bands (Hansen, 1997). Solid CO_2 also exhibits a strong absorption continuum at ultraviolet wavelengths of 50–130 nm (Warren, 1986). It is therefore conceivable that there could be a considerable difference in the *e*-folding scale of snow made from these optically very different materials. The optical properties of solid CO_2 are wavelength dependent and, as a consequence, so are the albedo and emissivity. However, according to Warren et al. (1990), the most important factors controlling the radiative properties are grain size and dust contamination of the snowpack. The added complication when considering light penetration in snow over solid ice is the large number of scattering surfaces, resulting in light propagation being dependent upon both transmission through the ice and reflections at grain boundaries. This means that many other factors, such as grain size, shape, and density of the snowpack, need to be considered in addition to the optical properties of the ice itself.

The combination of all of these factors shows the importance of broad wavelength range light penetration measurements, of both pure CO_2 and H_2O snow, in order to accurately determine the penetration depth of solar light. These measurements could lead to more accurate models of radiative transfer at the Martian surface, which could improve estimates of CO_2 snow deposition (such as those by Forget et al.

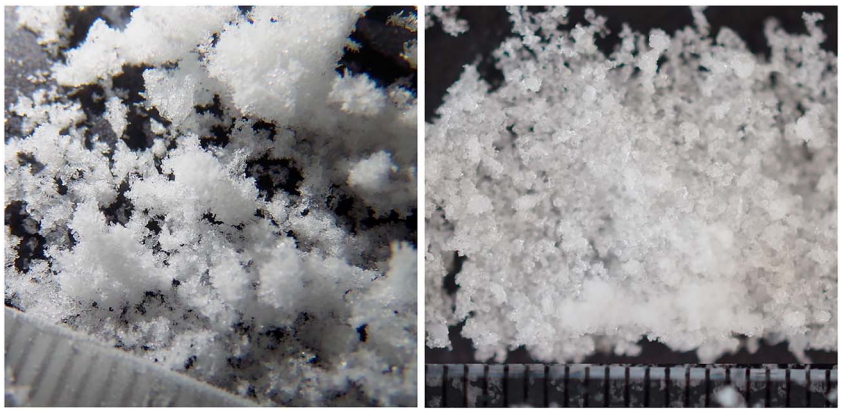

Figure 1. Freshly made CO_2 snow (left) and H_2O snow (right). Upon visual inspection it is difficult to tell the two materials apart. Both ices, when formed using our method, consist of fine granular material, which appears white and fluffy. The scale on the ruler in both images is in millimeters.

(1998)), subsnow surface temperatures, and snow-covered shallow subsurface heat flow gradients, all of which lead to a better understanding of the dynamic Martian surface.

2. Methodology

2.1. Snow Preparation

CO_2 snow was made using an Air Liquide Snowpack maker, connected directly to a liquid CO_2 cylinder. The snow was then immersed in liquid nitrogen, which caused immediate disintegration of the snowpack, and ensured homogenous, fine-grained snow, similar to the methodology of Kossacki et al. (1997). The suspension was then poured through a sieve to remove the snow from liquid nitrogen. At this point, the snow was around the temperature of liquid nitrogen and was stored in sealed bags kept in an insulated polystyrene container in a freezer at 187 K for the duration of the experiments (around 2–3 hr in total), extracting only the quantity required for each experimental run. Due to the presence of some remaining liquid nitrogen in the container, the snow remained cold enough to prevent sintering, which would have caused the snow to clump and make it difficult to work with, invalidating the results.

Water snow was made by spraying deionized water into a dewar of liquid nitrogen. Once a sufficient amount of snow had formed in the bottom of the dewar the liquid nitrogen was then poured through a sieve (1.18-mm mesh size) to remove any larger ice chunks from the snow. As with the CO_2 snow, this was kept in sealed bags within an insulated box in the deep freezer and used on the day of production, in order to avoid sintering. The resulting snow samples, both CO_2 and H_2O, can be seen in Figure 1.

Once made, the water snow was sieved using a range of standard sample sieve sizes, in order to determine if there was any grain size dependence on the *e*-folding scale. Note that, in this context, "grain size" refers to conglomerates of small ice granules rather than grains of compact ice (see section 3). Figure 1 shows the typical structure of our snow. In order to investigate grain size dependence of light transmission through compact ice, a different production mechanism for the grains would have to be used. The sieves were pre-cooled, and sieving was performed in a freezer, with the different snow samples immediately bagged and stored back in the freezer. The intention had been to repeat this process with CO_2 snow. However, due to the rapid sintering rates, and requirement for the sieves to be kept below the freezing point of CO_2, the process rendered the sample unusable for these experiments. Therefore, we conducted a grain size analysis on three separate samples of CO_2 snow prepared using identical methodology to that used in the experiments and used the proportional grain sizes to be representative of each new snow batch made. The proportional grain size distribution within each CO_2 snowpack sieved and weighed can be seen in Figure 2.

Both the CO_2 and H_2O snow experiments were undertaken in an argon-filled chamber, which is first cooled with liquid nitrogen (shown in Figure 4). This both reduced the sublimation rate of the CO_2 ice and minimized water frost deposition on both the sample and the glass plate the sample is placed on.

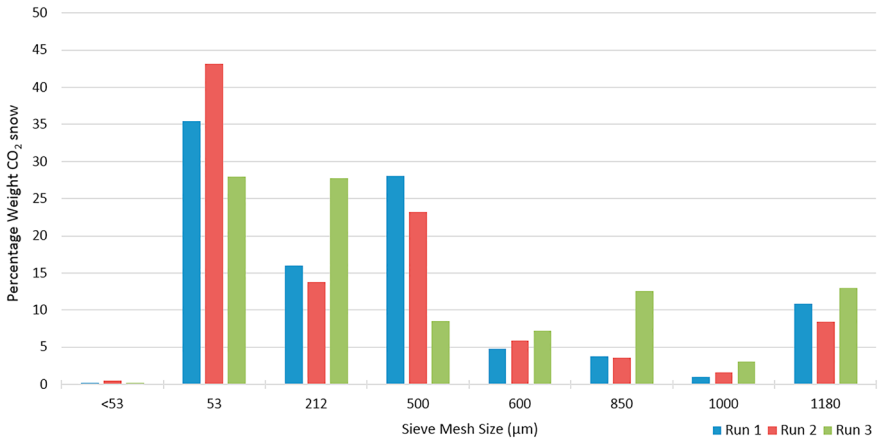

Figure 2. Representative grain size distribution in CO_2 snowpacks using our methodology. Note that even a large a snow "grain" can consist of hundreds of minuscule ice granules only a few tens of micrometers in diameter.

Throughout these experiments, all samples are freshly prepared and stored for as short a time as possible, under conditions that minimize the possibility of sintering. This is particularly problematic with CO_2 snow, due to its low freezing point. When a substance condenses as a fluffy, fine-grained deposit such as snow, sintering occurs in order achieve the preferred thermodynamic state of minimum surface energy (Eluszkiewicz, 1993). Therefore, sintering results in grain growth and densification. As a consequence, the optical path length through the grains increases, thus reducing the number of scattering surfaces over a fixed volume. This would therefore have a significant impact on the *e*-folding scale of the material. This process can be seen in Figure 3, through leaving a batch of snow to sinter for increasing amounts of time, in a sealed container placed in the freezer at 187 K. In the final/lower-right image, the residual grain outlines can still be seen, where the individual grains have grown via vapor diffusion, and eventually joined up.

2.2. Experimental Setup

The experimental setup is shown in Figure 4. The sample was irradiated using a full spectrum solar simulator (LS1000R3, Solar Light Company), with the beam directed via a mirror to penetrate the sample perpendicular to the surface of sample, which was scraped flat and smooth. The transmitted irradiation was then measured using a pyranometer (CS300, Campbell Scientific Ltd.) sensitive to wavelengths from 300 to 1,100 nm (absolute accuracy ±5% for daily total radiation). Prior to the experiment commencement the beam intensity was measured with the pyranometer to monitor consistency, although it is important to note that our *e*-folding scale measurements are independent of total irradiance.

The experiment chamber and contents (including glass plate which the sample was placed on and the scraper) were precooled prior to experiment commencement by use of the cooled argon. If these were cooled in the freezer separately, while they may be colder, they would immediately frost up when removed from the freezer and placed in the chamber. Some lumps of CO_2 snow were also placed in the bottom of the chamber, away from the pyranometer, in order to facilitate more efficient cooling at this initial stage. These had completely sublimated by the time experiments were under way. There was no specific temperature control other than to cool the system as much as possible.

2.3. Experimental Procedure

Reliable albedo measurements for thin samples are difficult to obtain and are often of poor accuracy due to the measurements being influenced more by the albedo of the underlying surface than the sample being measured (Wiscombe & Warren, 1980). Consequently, in order to avoid these additional uncertainties, a minimum thickness of 5 mm of snow is used in all of these experiments. This is then taken as the zero point for the calculation of the *e*-folding scale, with all measurements normalized accordingly. This is consistent with the methods of Kaufmann and Hagermann (2015), who used a minimum snow thickness of 5 mm for their measurements.

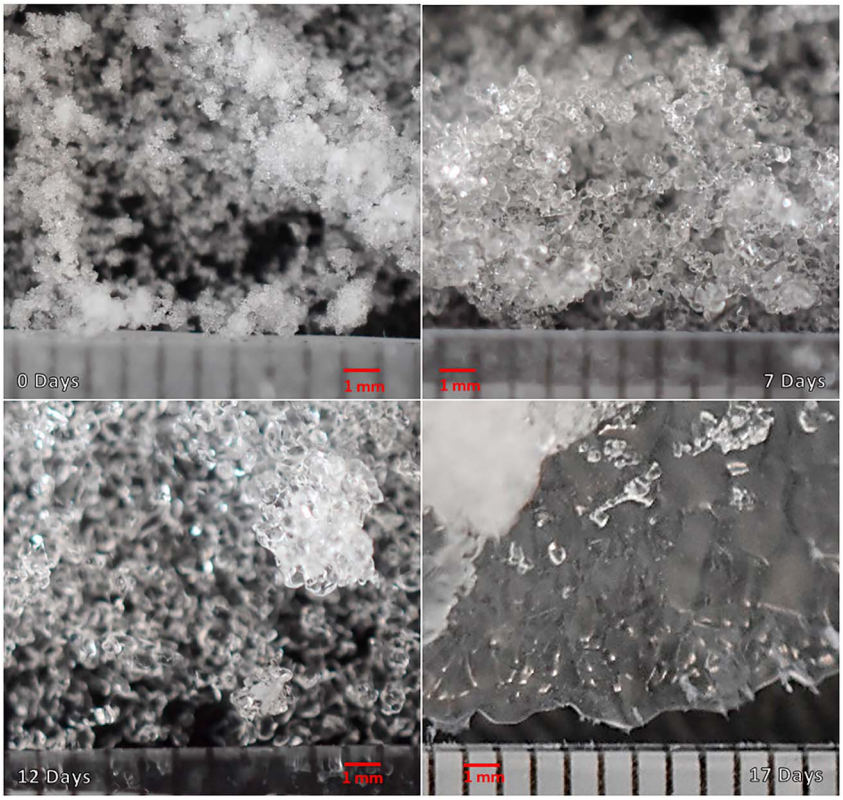

Figure 3. From top left to bottom right: Freshly made CO_2 snow, CO_2 snow left in the freezer at 187 K for 7 days, CO_2 snow left in freezer for 12 days, CO_2 snow left in freezer for 17 days. Over time the very fine grains of snow in the first image gradually grow in size and joint up until forming solid sheets of ice several centimeters in length, in the 17 days image (bottom right).

A series of copper rings 86 mm in diameter (painted black on the inside to prevent internal reflections) were used to contain the snow samples at set thicknesses. This ensured consistent volumes of snow and made reducing the thickness of the snowpack for consecutive measurements quick and accurate. The sample was placed inside the chamber, the solar simulator lamp turned on, and first light intensity measurement taken. The shutter was closed on the solar lamp between measurements in order to minimize sublimation and sintering. For water snow, four measurements are made per snow thickness, one in the center and three further measurements at different locations in the sample offset from the center. This is in order to reduce the effect of any slight inhomogeneities present within the sample. However, due to the rapid sintering rate of CO_2 snow just one measurement per snow thickness could be made.

The top copper ring was then removed and the snow sample gently scraped smooth along the level of the underlying copper ring with the flat edge of a plastic spatula to the next required thickness. This was conducted while inside the chamber and flooded with cooled argon. The lamp was then unshuttered in order to take the next measurement, and the process repeated as swiftly as possible. Bohren and Barkstrom (1974) suggested that light transmission experiments in snow should made using a sample container whose diameter is at least twice the maximum sample thickness, in order for any interference from the walls on the sample to be negligible. Therefore, the maximum snow thickness used for any measurements was 35 mm (to ensure this effect is minimized completely). In addition, like Kaufmann and Hagermann (2015), it was found that the larger the snow sample, the greater the errors induced from a number of sources. Therefore, in order to minimize the error of sample thickness measurement, maximize the amount of energy analyzed by the pyranometer, and minimize errors introduced by secondary reflections from and diffuse scattering within the sample, measurements were mainly taken over 15 mm, and the results exclusively calculated over this range. Measurements were taken through samples at 15, 10, and 5 mm for both water and carbon dioxide snows.

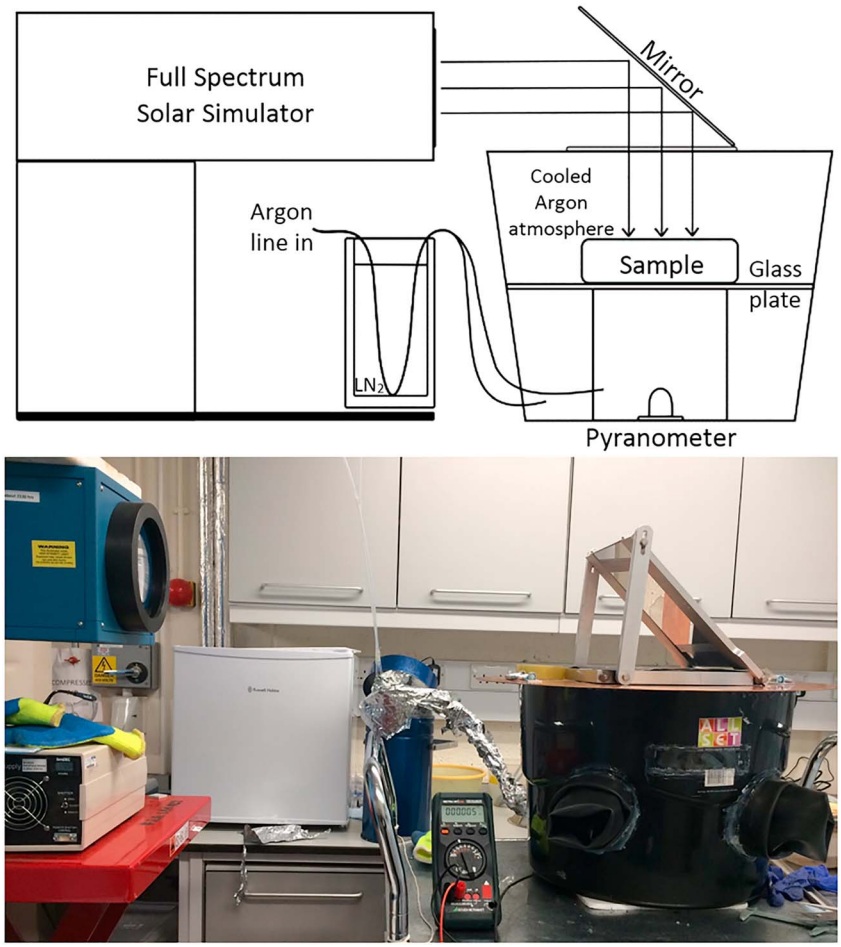

Figure 4. Schematic of experimental setup for CO_2 ice *e*-folding scale measurements (top), and photograph of the same set up in the lab (bottom).

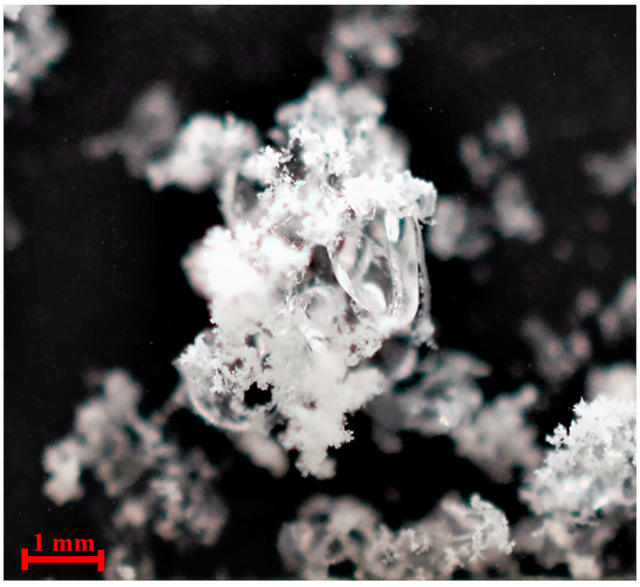

Figure 5. Water frost forming on larger grains of translucent carbon dioxide ice when exposed to air.

Each sample was weighed prior to irradiation commencement, and so the initial density of each snowpack has been calculated for both H_2O and CO_2 snow. It was not possible to weigh the samples in between irradiation events at each thickness, as this would have exposed the samples to warmer temperatures and humidity, accelerating sintering rates and increasing the amount of water frost contamination in CO_2 snow samples (an example of which can be seen in Figure 5), and melting in the water snow samples. It was particularly important to prevent melting of the water snow, as not only does liquid water have a different refractive index to ice, water pooling in between snow grains would essentially increase the optical path length by joining up grains with an optically similar material (ice/air boundary compared to ice/water boundary) and so will cause much less scattering, and therefore less attenuation, than without the liquid phase. Efforts were made at each reduction of snow thickness to only scrape the surface level without compacting the snowpack, although it is acknowledged that some small amount of compaction may have occurred.

Cooled argon continuously flowed into the chamber in an attempt to mitigate the formation of water frost on both the samples of CO_2 snow, and on the glass plate suspending the samples above the pyranometer.

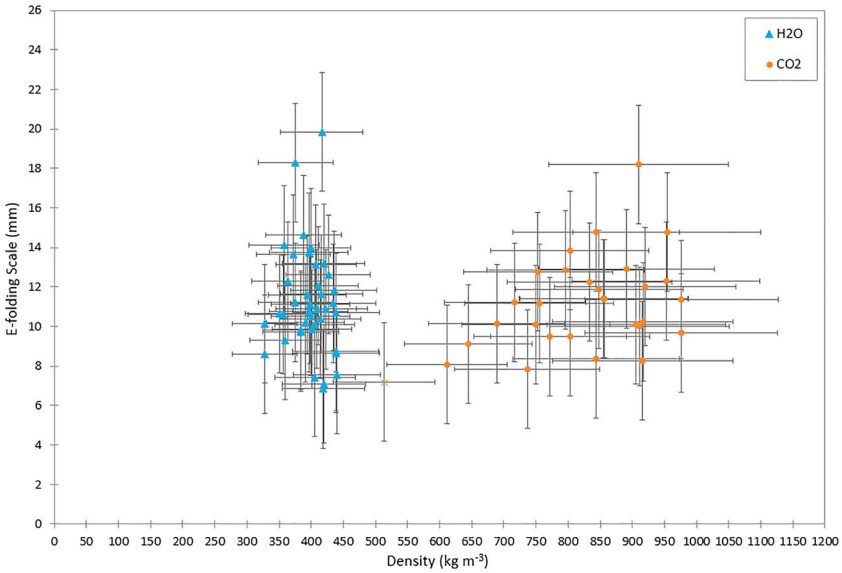

Figure 6. The *e*-folding scale results plotted with snowpack starting density. The data point denoted by the orange cross was an initial run with CO_2 snow, which enabled the experimental set up to be refined. This practice run was excluded from further analyses of this data. Errors in the density measurements (horizontal error bars) are calculated based on measuring equipment tolerances, and the vertical errors for the *e*-folding scale account for both equipment tolerances and potential human error introduced when scraping each ice thickness flat.

3. Results

Light intensity measurements made through CO_2 and H_2O snow samples of different thicknesses were conducted using an identical experimental set up, and the results used to calculate the *e*-folding scale, or penetration depth, of each material. These were made using a broad wavelength range across the visible spectrum (300–1100 nm). Figure 6 shows how the *e*-folding scale varies with density. A practice run was made to test the initial experimental setup and, for the sake of completeness, is also plotted and denoted by an orange cross. Several alterations to the setup were made based on this measurement, which included improvements to reduce air leakage into the chamber, and flooding the chamber with cooled argon to prevent the formation of water frost.

The *e*-folding scale is calculated from the raw light intensity measurements by first adjusting the data for the 5-mm measurement to be taken as the zero depth to remove the effect of albedo (as previously discussed). All data are then normalized accordingly, and by rearranging equation (1), the *e*-folding scale (ζ) is then calculated. The full data sets of raw light intensity measurements for both CO_2 and H_2O snows are available in the supporting information provided alongside this manuscript. As water snow measurements have 4 data points for each sample thickness, the raw light intensity readings were averaged for each snow depth prior to calculating the *e*-folding scale. The results are plotted in Figure 6, where is can be seen that there is a very weak correlation of higher *e*-folding scale with increased density, although this is less evident in the H_2O snow data than in CO_2 snow.

The density of CO_2 snow on Mars has been constrained to 910 ± 230 kg/m^3 based on data from the Mars Orbiter Laser Altimeter on the Mars Global Surveyor (Smith et al., 2001), a range which is covered by our measurements. Our results suggest that the *e*-folding scale does not vary significantly through the density range. This seems to be consistent with previous studies measuring other optical properties of water snow; Bohren and Beschta (1979) found that if grain size was kept constant, then there was no significant change in albedo with compaction (an average 1 percentage point decrease in albedo for compacted snow, not significant at the 90% confidence level).

The mean *e*-folding scale of water snow was found to be 11.24 mm, and 11.25 mm for CO_2 snow (excluding the practice run). This result was unexpected given that the optical properties of these two materials are quite different. Additionally, the reported *e*-folding scale for H_2O and CO_2 slab ice has quite a large

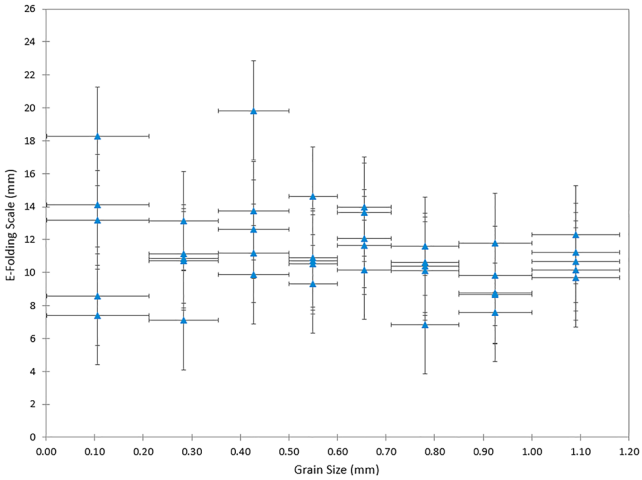

Figure 7. The *e*-folding scale results for water snow, dependent on snow grain size. Snow grains larger than 1.18 mm were deemed too big to be defined as "snow" and so are not used for these analyses. Horizontal error bars simply denote the range of grain sizes contained within that sample. Vertical errors here are based on the experimental error, including device tolerance and human error.

variation: the measurements made by Chinnery et al. (2018) report the *e*-folding scale of CO_2 slab ice varied from 35 to 65 mm depending upon the state of the ice sample, such as the extent of cracking or "milkiness" of the ice; no broad spectrum penetration depth measurements for water ice have been found in the literature, however, those made at discreet wavelength ranges show orders of magnitude differences based on wavelength: *e*-folding scales decrease sharply from 24 m at $\lambda = 470$ nm, to 8 m at $\lambda = 600$ nm, 2 m at $\lambda = 700$ nm, $\lambda = 0.05$ m at 1,000 nm, and $\lambda = 0.006$ m at 1,400 nm (Perovich, 1996). However, we propose that for small grain sizes such as snow, such a small amount of light transmission occurs through the ice grains that the material properties have a negligible effect and light transmission is dominated by scattering/multiple reflections between grains. This suggests that at these very small scales, grain morphology and the number of scattering surfaces is more important than snow composition.

This interpretation is further supported by the data represented in Figure 7. Artificial water snow can be kept pure and stable much more easily than CO_2 snow, and so grain size dependence was tested using only water snow. If this had been attempted with CO_2 snow then sintering and H_2O frost accumulation would have occurred during the multiple sieving steps required, rendering the samples unusable. The snow was prepared and sieved as outlined in the methodology section, and light transmission was measured on discreet grain size ranges. It can be seen that there is no discernible trend linking *e*-folding scale with grain sizes at this small scale, although it should be noted that scatter in the data increased with decreasing snow grain size.

Upon close scrutiny of the water snow, which had been sieved to discrete grain sizes, it could be seen that the "grains" actually appeared to consist of clumps of even smaller granules. It is therefore perhaps more accurate to describe the grain size ranges by using only the upper boundary. While a finer meshed sieve was also used to define the lower limit of the grain size range, it cannot be conclusively said that smallest individual grains are larger than this, only that the smallest clumps of grains are at least this size. This can be seen in Figure 8, for the grain size range 0.71–0.85 mm.

Based on these observations, it is impossible to tell whether these granular conglomerates behave optically as one unit, or as the individual constituents, scattering light at each internal surface. It would be reasonable to assume a range of behavior with regard to this, depending on the extent to which the conglomerate grain has fused together. It should, however, be noted that the snow used for the actual measurements was kept at consistently lower temperatures than the sample shown here, which would have warmed, and therefore

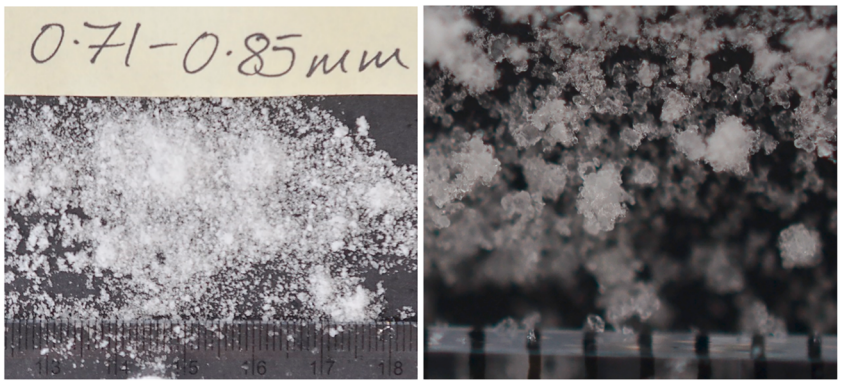

Figure 8. Water snow sieved to grain sizes between 0.71 and 0.85 mm. On initial inspection the grain size range appears entirely reasonable (left). However, when inspected at closer range (right), noting the scale shown on both images is in millimeters, clusters of grains much smaller than 0.71 mm can be seen clustered together forming conglomerates which appear to fall within the desired grain size range.

likely sintered, to a greater extent during the process of photographing it. This suggests one contributing factor as to why, in the data presented here (Figure 7), we observe no significant trend between the penetration depth and grain size, despite theoretically being expected. In addition to this, Chinnery et al. (2018) found the *e*-folding scale of CO_2 slab ice to vary from around 35 to 65 mm, the upper limit being for near-pristine slabs, and the lower for highly cracked imperfect ice, reducing the effective grain size or path length between cracks. It seems most likely, due to the difficulties in constraining the grain sizes by sieving, that the large range of actual grain sizes make it difficult to discern a trend in the data.

Beaglehole et al. (1998) conducted light transmission experiments in naturally formed Antarctic snow and modeled their results using spherical snowparticles and two flux theory, which showed that while the absorption coefficient should scale with relative density, the scattering coefficient should scale inversely with grain size. This explains our observation of little density dependence in the *e*-folding scale results from these measurements of snow grains <1.18 mm, and why is it the same regardless of composition, as little absorption is occurring. However, it also implies that there should be strong grain size dependence. We suggest that this trend is obscured by uncertainties in determining the minimum grain size range for each snow sample, as discussed above. Combined with the relatively small range of grain sizes analyzed, this results in inherent errors which are larger than the amplitude of any trend which could have been recorded. A more extensive range of measurements covering a much larger range of ice grain sizes, formed using compact ice, would be required to determine the underlying cause of these observations.

4. Discussion

The snow used for the *e*-folding scale experiments by Kaufmann and Hagermann (2015) was made by an industrial snow cannon, and was later found to contain some contaminants. This is acceptable for determining the effect of dust contamination, as it was the only variable in the system, but not so accurate for determining the *e*-folding scale of pure water snow. We believe Kaufmann & Hagermann's value of 5.4 ± 1 mm to be too low because the effect of contaminants generally decreases the *e*-folding scale. France et al. (2010) also conducted light intensity measurements through pure and dust contaminated snowpacks. Conversely, they generated their water snow by spraying pure water into a bath of liquid nitrogen, similar to the methodology used in our study presented here, meaning the snow was free of contaminants. However, the samples were then left to sinter for 24 hr at 253 K, which would result in a not insignificant degree of sintering. Sintering is the process of grains both growing and in part fusing together followed by snowpack densification, thus increasing the path length which light propagates through the snow. This goes some way to explaining why their *e*-folding scale is an order of magnitude greater than that measured by Kaufmann and Hagermann (2015). By contrast, the samples for our measurements were always freshly prepared—and did not contain any impurities. It should also be noted that France et al. (2010) used discrete wavelengths from 400 to 700 nm, whereas the measurements presented here are across the broader wavelength range of the pyranometer (300–1100 nm), which could also explain some discrepancy in the results. This is demonstrated by the vast range of *e*-folding scales of sea ice reported by Perovich (1996) and discrete wavelength ranges, from 24 m at $\lambda = 470$ nm, decreasing dramatically to 5 cm at $\lambda = 1000$ nm.

A sophisticated model of solar radiation penetration in CO_2 ice was created by Pilorget et al. (2011), which combined both radiative and conductive heat transfer methods with the optical properties of carbon dioxide ice. The findings presented in this manuscript are consistent in principle with these model results, in that small grains of CO_2 ice, of a size classed as snow throughout this study, do now allow enough light to penetrate through a layer to allow for any significant heating of the underlying regolith. What this study did not provide, however, were the resultant penetration depths for CO_2 ice in the different scenarios modeled.

The implications of such a small *e*-folding scale for fine-grained ices are that if there is even a small amount of snow cover on top of the seasonal ice slab, which it is reasonable to suggest could remain suitably cold so as to not cause rapid sintering of the snow, then light penetration into the ice sheet could be dramatically dampened. This would hamper the formation of araneiforms, for example, which only occur when adequate energy can be transmitted through the ice to the underlying regolith. This is in order to heat the regolith sufficiently to cause basal sublimation which leads to CO_2 jetting, as per the CO_2 jetting model (Kieffer, 2000, 2007; Kieffer, et al., 2006, etc.). Perovich (1996) states that, on Earth, a 25-cm covering of snow on top of an ice sheet would reduce light transmittance to less than 1%. While this would be a very large amount of CO_2

snow to accumulate on Mars, the simulations run by Colaprete (2002) indicate that 0.75 g of CO_2 snow could be deposited per square centimeter during 1 hr of snowfall beneath the CO_2 clouds forming the polar hood. If using a snow density of 910 kg/m^3 (Smith et al., 2001), this equates to 8.2-mm-thick deposit of snow, and given the *e*-folding depth of 11.2 ± 3 mm, even at these lesser snow depths a significant reduction in radiation intensity will occur, potentially halting the CO_2 jetting process while the snow remains in situ. This would not even necessarily require snow fall to emplace fine-grained ice deposits. One of the issues raised by Pilorget et al. (2011) was that CO_2 jetting was observed on dune slopes but not on the flat areas between dunes. They suggested that venting was still occurring in these areas, but the underlying regolith on the flat areas has a higher albedo than that of the dune material and so made it harder to observe. In addition to the issue of detection, it could also be speculated that if fine-grained icy debris ejected from the vents on the dune slopes were carried downslope (either simply by gravity or windblown) and deposited around the foot of the dune, that the presence of even a very thin layer of granular ice on top of the slab ice, combined with the higher albedo regolith (therefore less absorbing) could be enough to suppress jetting activity.

CO_2 sublimation processes have also been linked to the formation of gullies in the absence of liquid water (e.g., Cedillo-Flores et al., 2011; Hoffman, 2002; Pilorget & Forget, 2015; Vincendon, 2015). These are mainly found in the 30–60° latitude range in both hemispheres, and activity has been linked to the time when seasonal CO_2 frost is present on the surface and beginning to defrost (Pilorget & Forget, 2015). In a series of laboratory experiments, Sylvest et al. (2018) condensed CO_2 frost onto JSC Mars-1 simulant regolith, held at angles ranging from 10° through to the angle of repose, in order to investigate gully formation when exposed to incident radiation. They found that the CO_2 formed as fine-grained deposits on the surface, and between the regolith grains. Significant thicknesses of CO_2 frost (up to several centimeters) can accumulate on pole-facing slopes even at mid-latitudes, even though these are illuminated by the sun (Schorghofer & Edgett, 2006).

An *e*-folding scale of only 1.1 cm in snow would mean that the underlying material, be it regolith or ice, is largely unaffected by insolation—and thus might remain colder than anticipated. Lower subsurface temperatures reduce gas movement through the pores in a sediment, affecting both the subsurface-atmosphere exchange of CO_2 and the likelihood of sediment movement to be triggered by CO_2 sublimation. Lower subsurface temperatures also affect the sublimation of other volatiles potentially present in the subsurface, such as water, increasing the survival time of any subsurface water ice deposits.

5. Conclusions

The *e*-folding scale of fresh, unsintered water snow and carbon dioxide snow have been measured across the wavelengths 300 to 1100 nm and found to be $\zeta = 11 \pm 3$ mm, regardless of composition, for grains <1.18 mm. This has applications for use in radiative transfer models applied to Mars and other icy surfaces in the solar system where fine-grained ice or snow is present. Although snow may only fall at isolated locations and times of year, there is a widespread, low-latitude, and year-round frost cycle for which this work is also applicable. While water and carbon dioxide ices have different optical properties, and in massive, or slab ice form, they have different *e*-folding scales, for grain sizes <1.18 mm, the large amount of scattering surfaces based on the grain morphology is a more important factor than ice composition, making internal reflections within the snowpack the dominant light transfer mechanism over transmission through the ice grains. As snow sinters and compacts over time, light propagation through the ice will transition from being dominated by scattering, to an increase in propagation through the ice until it *e*-folding scales of slab ice are more applicable, which differ based on composition. This shows that, while it is important to be able to define the composition of solid ice to determine the thermal regime of the surface, if there is snow cover, the composition of that snow does not affect the penetration depth of broad wavelength solar radiation. This could simplify the incorporation of surface CO_2 snow cover into models, as this had previously been approximated to either exhibit the same behavior as CO_2 clouds, as in Forget et al. (1998), or has been calculated theoretically for a given wavelength and single grain size, using CO_2 optical properties in a combination Mie theory and the Delta-Eddington method for scattering in a snowpack (e.g., Pilorget et al., 2011). In order to understand the transition from light transmission in snow to that in slab ice, a more extensive range of measurements covering a much larger range of ice grain sizes would be required. Results from this would

also give insights on how snow which has begun sintering would behave, with grain sizes increasing until slab ice is formed.

While this has obvious implications for the Martian surface (where both water and carbon dioxide snow and granular ice has been detected) wherever ices are present on a surface, such as comets or icy moons, with incident solar irradiation a solid-state greenhouse will be induced, and so the *e*-folding scale of that ice will be an important parameter to define.

Acknowledgments
The authors would like to thank Ganna Portyankina and two further anonymous reviewers for their comments and suggestions that have greatly improved this manuscript. This work was funded by STFC under grant ST/N50421X/1 with additional support from grants ST/S001271/1 and ST/P000657/1, as well as UKSA grants ST/R001405/1 and ST/S00145X/1. Access to the full data set generated in these experiments can be found in the supporting information.

References

Arvidson, R. E., Bonitz, R. G., Robinson, M. L., Carsten, J. L., Volpe, R. A., Trebi-Ollennu, A., et al. (2009). Results from the Mars Phoenix Lander Robotic Arm experiment. *Journal of Geophysical Research*, *114*, EO0E02. https://doi.org/10.1029/2009JE003408

Beaglehole, D., Ramanathan, B., & Rumberg, J. (1998). The UV to IR transmittance of Antarctic snow. *Journal of Geophysical Research*, *103*(D8), 8849–8857. https://doi.org/10.1029/97JD03604

Bohren, C. F., & Barkstrom, B. R. (1974). Theory of the optical properties of snow. *Journal of Geophysical Research*, *79*(30), 4527–4535. https://doi.org/10.1029/JC079i030p04527

Bohren, C. F., & Beschta, R. L. (1979). Snowpack albedo and snow density. *Cold Regions Science and Technology*, *1*(1), 47–50. https://doi.org/10.1016/0165-232X(79)90018-1

Cedillo-Flores, Y., Treiman, A. H., Lasue, J., & Clifford, S. M. (2011). CO_2 gas fluidization in the initiation and formation of Martian polar gullies. *Geophysical Research Letters*, *38*, L21202. https://doi.org/10.1029/2011GL049403

Chinnery, H. E., Hagermann, A., Kaufmann, E., & Lewis, S. R. (2018). The penetration of solar radiation into carbon dioxide ice. *Journal of Geophysical Research: Planets*, *123*, 864–871. https://doi.org/10.1002/2018JE005539

Clark, R. N., Fanale, F. P., & Zent, A. P. (1983). Frost grain size metamorphism: Implications for remote sensing of planetary surfaces. *Icarus*, *56*(2), 233–245. https://doi.org/10.1016/0019-1035(83)90036-2

Colaprete, A. (2002). Carbon dioxide snow storms during the polar night on Mars. *Journal of Geophysical Research*, *107*(E7), 5051. https://doi.org/10.1029/2001JE001758

Cull, S., Arvidson, R. E., Mellon, M., Wiseman, S., Clark, R., Titus, T., et al. (2010). Seasonal H_2O and CO_2 ice cycles at the Mars Phoenix landing site: 1. Prelanding CRISM and HiRISE observations. *Journal of Geophysical Research*, *115*, E00D16. https://doi.org/10.1029/2009JE003340

Eluszkiewicz, J. (1993). On the microphysical state of the Martian seasonal caps. *Icarus*, *103*, 13–48. https://doi.org/10.1006/icar.1993.1056

Eluszkiewicz, J., Moncet, J.-L., Titus, T. N., & Hansen, G. B. (2005). A microphysically-based approach to modeling emissivity and albedo of the Martian seasonal caps. *Icarus*, *174*(2), 524–534. https://doi.org/10.1016/j.icarus.2004.05.025

Forget, F., Hourdin, F., & Talagrand, O. (1998). CO_2 snow fall on Mars: Simulation with a general circulation model. *Icarus*, *131*(2), 302–316. https://doi.org/10.1006/icar.1997.5874

France, J. L., King, M. D., & MacArthur, A. (2010). A photohabitable zone in the Martian snowpack? A laboratory and radiative-transfer study of dusty water–ice snow. *Icarus*, *207*(1), 133–139. https://doi.org/10.1016/j.icarus.2009.11.026

Genova, A., Goossens, S., Lemoine, F. G., Mazarico, E., Neumann, G. A., Smith, D. E., & Zuber, M. T. (2016). Seasonal and static gravity field of Mars from MGS, Mars odyssey and MRO radio science. *Icarus*, *272*, 228–245. https://doi.org/10.1016/j.icarus.2016.02.050

Gillmann, C., Lognonné, P., Chassefière, E., & Moreira, M. (2009). The present-day atmosphere of Mars: Where does it come from? *Earth and Planetary Science Letters*, *277*(3–4), 384–393. https://doi.org/10.1016/j.epsl.2008.10.033

Hansen, G. B. (1997). The infrared absorption spectrum of carbon dioxide ice from 1.8 to 333 μm. *Journal of Geophysical Research*, *102*(E9), 21569–21587. https://doi.org/10.1029/97je01875

Hayne, P. O., Paige, D. A., & Heavens, N. G. (2014). The role of snowfall in forming the seasonal ice caps of Mars: Models and constraints from the Mars Climate Sounder. *Icarus*, *231*, 122–130. https://doi.org/10.1016/j.icarus.2013.10.020

Hayne, P. O., Paige, D. A., Schofield, J. T., Kass, D. M., Kleinböhl, A., Heavens, N. G., & McCleese, D. J. (2012). Carbon dioxide snow clouds on Mars: South polar winter observations by the Mars Climate Sounder. *Journal of Geophysical Research*, *117*, E08014. https://doi.org/10.1029/2011JE004040

Hoffman, N. (2002). Active polar gullies on Mars and the role of carbon dioxide. *Astrobiology*, *2*(3), 313–323. https://doi.org/10.1089/153110702762027899

Kaufmann, E., & Hagermann, A. (2015). Penetration of solar radiation into pure and Mars-dust contaminated snow. *Icarus*, *252*, 144–149. https://doi.org/10.1016/j.icarus.2015.01.007

Kieffer, H. H. (2000). Annual Punctuated CO2 Slab-Ice and Jets on Mars. *International Conference on Mars Polar Science and Exploration* (93 pp.), Mars Polar Science: 4095.

Kieffer, H. H. (2007). Cold jets in the Martian polar caps. *Journal of Geophysical Research*, *112*, E08005. https://doi.org/10.1029/2006JE002816

Kieffer, H. H., Christensen, P. R., & Titus, T. N. (2006). CO2 jets formed by sublimation beneath translucent slab ice in Mars' seasonal south polar ice cap. *Nature*, *442*(7104), 793–796.

Kossacki, K. J., Kömle, N. I., Leliwa-Kopystynski, J., & Kargl, G. (1997). Laboratory investigation of the evolution of cometary analogs: Results and interpretation. *Icarus*, *128*(1), 127–144. https://doi.org/10.1006/icar.1997.5701

Kuroda, T., Medvedev, A. S., Kasaba, Y., & Hartogh, P. (2013). Carbon dioxide ice clouds, snowfalls, and baroclinic waves in the northern winter polar atmosphere of Mars. *Geophysical Research Letters*, *40*, 1484–1488. https://doi.org/10.1002/grl.50326

Leighton, R. B., & Murray, B. C. (1966). Behavior of carbon dioxide and other volatiles on Mars. *Science*, *153*(3732), 136–144. https://doi.org/10.1126/science.153.3732.136

Matson, D. L., & Brown, B. H. (1989). Solid-state greenhouses and their implications for icy satellites. *Icarus*, *77*(1), 67–81. https://doi.org/10.1016/0019-1035(89)90007-9

Möhlmann, D. T. F. (2010). Temporary liquid water in upper snow/ice sub-surfaces on Mars? *Icarus*, *207*(1), 140–148. https://doi.org/10.1016/j.icarus.2009.11.013

Niederdorfer, E. (1933). Messungen des Wärmeumsatzes über schneebedecktem Boden. *Meteorologische Zeitschrift*, *50*, 201–208.

Perovich, D. K. (1996). *The optical properties of sea ice*. In J. Richter-Menge & G. Maykut (Eds.), *CRREL Monograph 96–1*, edited. Springfield, VA: Office of Naval Research.

Pilorget, C., & Forget, F. (2015). Formation of gullies on Mars by debris flows triggered by CO_2 sublimation. *Nature Geoscience*, *9*(1), 65–69.
Pilorget, C., Forget, F., Millour, E., Vincendon, M., & Madeleine, J. B. (2011). Dark spots and cold jets in the polar regions of Mars: New clues from a thermal model of surface CO_2 ice. *Icarus*, *213*(1), 131–149. https://doi.org/10.1016/j.icarus.2011.01.031
Piqueux, S., Kleinböhl, A., Hayne, P. O., Heavens, N. G., Kass, D. M., McCleese, D. J., et al. (2016). Discovery of a widespread low-latitude diurnal CO_2 frost cycle on Mars. *Journal of Geophysical Research: Planets*, *121*, 1174–1189. https://doi.org/10.1002/2016JE005034
Schorghofer, N., & Edgett, K. S. (2006). Seasonal surface frost at low latitudes on Mars. *Icarus*, *180*(2), 321–334. https://doi.org/10.1016/j.icarus.2005.08.022
Smith, D. E., Zuber, M. T., & Neumann, G. A. (2001). Seasonal variations of snow depth on Mars. *Science*, *294*(5549), 2141–2146. https://doi.org/10.1126/science.1066556
Smith, P. H., Tamppari, L. K., Arvidson, R. E., Bass, D., Blaney, D., Boynton, W. V., et al. (2009). H_2O at the Phoenix landing site. *Science*, *325*(5936), 58–61. https://doi.org/10.1126/science.1172339
Snyder, C. W. (1979). The planet Mars as seen at the end of the Viking Mission. *Journal of Geophysical Research*, *84*(B14), 8487. https://doi.org/10.1029/JB084iB14p08487
Sylvest, M. E., Dixon, J. C., Conway, S. J., Patel, M. R., McElwaine, J. N., Hagermann, A., & Barnes, A. (2018). CO_2 sublimation in Martian gullies: Laboratory experiments at varied slope angle and regolith grain sizes. *Geological Society, London, Special Publications*, *467*, SP467.411. https://doi.org/10.1144/SP467.11
Titus, T. N., Kieffer, H. H., Mullins, K. F., & Christensen, P. R. (2001). TES premapping data: Slab ice and snow flurries in the Martian north polar night. *Journal of Geophysical Research*, *106*(E10), 23181–23196. https://doi.org/10.1029/2000je001284
Vincendon, M. (2015). Identification of Mars gully activity types associated with ice composition. *Journal of Geophysical Research: Planets*, *120*, 1859–1879. https://doi.org/10.1002/2015JE004909
Warren, S. G. (1982). Optical properties of snow. *Reviews of Geophysics and Space Physics*, *20*(1), 67–89. https://doi.org/10.1029/RG020i001p00067
Warren, S. G. (1986). Optical constants of carbon dioxide ice. *Applied Optics*, *25*(16), 2650–2674. https://doi.org/10.1364/AO.25.002650
Warren, S. G., Wiscombe, W. J., & Firestone, J. F. (1990). Spectral albedo and emissivity of CO_2 in Martian polar caps: Model results. *Journal of Geophysical Research*, *95*(B9), 14717. https://doi.org/10.1029/JB095iB09p14717
Wiscombe, W. J., & Warren, S. G. (1980). A model for the spectral albedo of snow. I: Pure snow. *Journal of the Atmospheric Sciences*, *37*(12), 2712–2733. https://doi.org/10.1175/1520-0469(1980)037<2712:AMFTSA>2.0.CO;2